University of Bath

Alternative formats
If you require this document in an alternative format, please contact:
openaccess@bath.ac.uk

Graphite-polydimethylsiloxane composite strain sensors for in-situ structural health monitoring

Alizé Vaihiria Gaumet[a], Richard J. Ball[b], Alain Nogaret[a,*]

[a]*Department of Physics and Centre for Nanoscience and Nanotechnology, University of Bath, Claverton Down, Bath, BA2 7AY, United Kingdom*
[b]*Department of Architecture and Civil Engineering, University of Bath, Claverton Down, Bath, BA2 7AY, United Kingdom*

Abstract

Here we describe the synthesis and testing of miniature sensors for structural health monitoring. The sensors were incorporated into building materials to detect strain relaxation events within the region of elastic deformation prior to the onset of plastic deformation. Our sensors consisted of thin composite films of polydimethylsiloxane and graphite nanoparticles that conduct via tunnelling percolation. Tunnelling-percolation through elastomers with low Young's modulus is highly sensitive to deformation and gives a large piezoresistance which we use to infer the local strain. The response of sensors embedded in calcium aluminate mortar, Portland cement mortar, and fine sand columns was compared under stress. We show that the sensors can detect micro-events where strain is redistributed locally from one direction to another and may thus be used to monitor structural integrity and provide early warning of material disaggregation.

Keywords: graphite, composite, strain gauge, tunnelling percolation, structural health monitoring

1. Introduction

The vulnerability of civil infrastructures and buildings to fatigue loading and chemical attack from the environment is driving the development of smart sensors that monitor structural health and provide a prior warning of damage which may otherwise lead to structural failure. Non-destructive evaluation methods [1, 2] are sought to activate the self-healing of construction materials [3–6] to mitigate against material disaggregation, and assist maintenance and rescue efforts. The strain sensors currently used to monitor built infrastructures are however large [7, 8] and expensive devices [7–9]. These are difficult to scale down to the level of the granular texture of concrete and to insert in building materials. Piezoresistive micro-sensors made of conductive elastomers would have the ability to detect the buildup of local strain thanks to their high sensitivity preserved down to the microscopic scale. They would also be well-suited for incorporation in sensing arrays that monitor disaggregation

---

*Corresponding author
Email address: `A.R.Nogaret@bath.ac.uk` (Alain Nogaret)

uniformly rather than at neuralgic points.

Composite films that are sensitive to local strain [10–25] have recently been developed for making artificial skins [14–18]. These incorporate conductive nanomaterials that include graphite particles [10–14], graphite nanosheets [22], graphene flakes [20, 21] or carbon nanotubes [15, 19, 24, 25] in a flexible insulating matrix. Addressable arrays with polydimethylsiloxane(PDMS)-based pixels have already been demonstrated to detect force fields with either current [18] or potential applications [19, 23] in the development of electronic skins. Piezoresistive arrays based on graphite-PDMS composite pixels have also been demonstrated to detect force fields to a degree of sensitivity (50Pa) comparable to the human touch [10]. The suitability of such composite sensors in the context of structural health monitoring remains to be assessed. This is the aim of the present work.

Here we synthesize millimetre-size composite sensors and embed them into construction materials to evaluate their suitability for detecting local strains which are currently inaccessible to existing strain gauges. Our sensors rely on tunnelling-percolation to obtain piezoresistance signals from which we extract the locally applied strain. The sensors were embedded in different cementitious materials to evaluate their response under a range of stress loadings. These materials include calcium aluminate mortar, Portland cement mortar, and fine sand columns. In each case, the local response of the composite sensor was compared to that of an external strain gauge as the samples were subjected to uniaxial stress. This work allowed us to assess the capability of our sensors at resolving local strain in-situ, improving structural health monitoring, as well as providing early warning of material disaggregation.

2. Principle of the tunnelling percolation strain sensor

The strain gauges used to monitor built infrastructures are large [7, 8] and expensive devices [7–9] that are difficult to scale down and embed in construction materials. This is particularly true for strain sensors based on optical interference gratings [26]. Piezoelectric strain sensors based on lead zirconium titanate ceramics (PZT) [2] include toxic materials such as lead and zirconium [27–29]. They are also fragile and lose sensitivity following damage [2]. In contrast, graphite-PDMS composite strain sensors would present several advantages including low cost, high sensitivity, scalability down to the size of individual graphite nanoparticles, industrial scalability allowed by their simple manufacturing process, as well as biocompatibility [10, 13].

The large piezoresistance of graphite-PDMS composites arises from their conduction mechanism based on tunnelling-percolation combined with the low Young modulus of the elastomer. Tunnelling-percolation describes hopping transport through a network of graphitic nanoparticles embedded in an insulating matrix. The hopping mechanism consists of tunnelling transmission through PDMS insulator with residual thermoelectric activation. In conventional percolation models, the vertices are either conducting or insulating. This all or nothing conductivity gives a clear percolation threshold. In contrast, tunnelling-percolation networks do not, a priori, have a percolation threshold since the tunnelling probability along vertices decays exponentially with the inter-particle distance. Because the conductivity of vertices never vanishes, it was not intuitively clear that network conductivity as a whole

would vanish at a finite value of the nanoparticle filling fraction. However Grimaldi and Balberg [30] have theoretically shown that a percolation threshold exists and that the network conductivity behaves similarly as a function of parameters as in conventional percolation. Taylor-Harrod et al. [11] have further computed the conductivity of a viscoelastic tunnelling-percolation network which is highly relevant to the graphite-PDMS composite. They have derived a formula for the piezoresistance of a composite film under biaxial strain. Given the similar mechanical boundary conditions and similar PDMS parameters (Young's modulus, Poisson modulus, viscosity) to the present experiment, the piezoresistance formula [11] approximates well the response of the present sensors to uniaxial stains smaller than 1%. The good match of the theoretically predicted and experimentally observed piezoresistance has been demonstrated by Chauhan et al. [10].

The sensitivity of the composite results from the exponential dependence of the tunnelling current on the distance between graphite nanoparticles hence the strain [10]. Under a compressive step, the average inter-particle distance decreases in the direction of the strain but increases in the transverse direction (Fig.1a). During the initial elastic response, the resistance of percolation paths increases giving a spike in the resistance. This is followed by a viscous relaxation phase where the composite relaxes into a state of lower resistance as transverse and longitudinal inter-particles separations converge to a lower average value (Fig.1b). In contrast, when the piezoresistive composite is subjected to hydrostatic pressure (Fig.1c), the tunnelling bond lengths decrease by the same amount in all three spatial directions. It follows that resistance decreases monotonically (Fig.1d). No resistance spike is observed as in the case of uniaxial strain.

The piezoresistance formula [11] uses the four following parameters: the chemical affinity of graphite, the visco-elastic creep time, the incomplete stress relaxation ratio and the volume filling fraction of graphite nanoparticles in the host material. We used this theory to compute the calibration curve of piezoresistance in response to incremental strain steps. We then used this calibration curve to convert the experimentally observed piezoresistance into the locally applied strain.

3. Materials and methods

3.1. Strain sensor

Our graphite-PDMS composite consists of highly oriented pyrolytic graphite (HOPG) nanoparticles of diameter 450nm (NanoAmor 1246HT) randomly dispersed in an insulating silicone matrix that is composed of a mixture of a polydimethylsiloxane rubber (Alchemie RTV 137) and a catalyst (Alchemie 137S). A volume filling fraction of 25% graphite nanoparticles was used in order to maximise strain sensitivity whilst allowing a reliable operation away from the percolation threshold (24%) [31]. We prepared the composite by first weighing pristine PDMS rubber and pouring it in a mortar. The appropriate mass of HOPG nanoparticles was then added to the rubber. Both components were then mixed together using pestle and mortar until a homogeneous mixture was obtained.

Separately, we fabricated a set of copper electrodes on a printed circuit board (PCB) to contact our composite film. The copper pads were fabricated through lithography and etching of the 35μm copper layer covering a single-sided photoresist board (300mm $\times$ 200mm $\times$ 0.4mm). Holes of 400μm diameter were drilled in each copper pad to drive through a 350μm
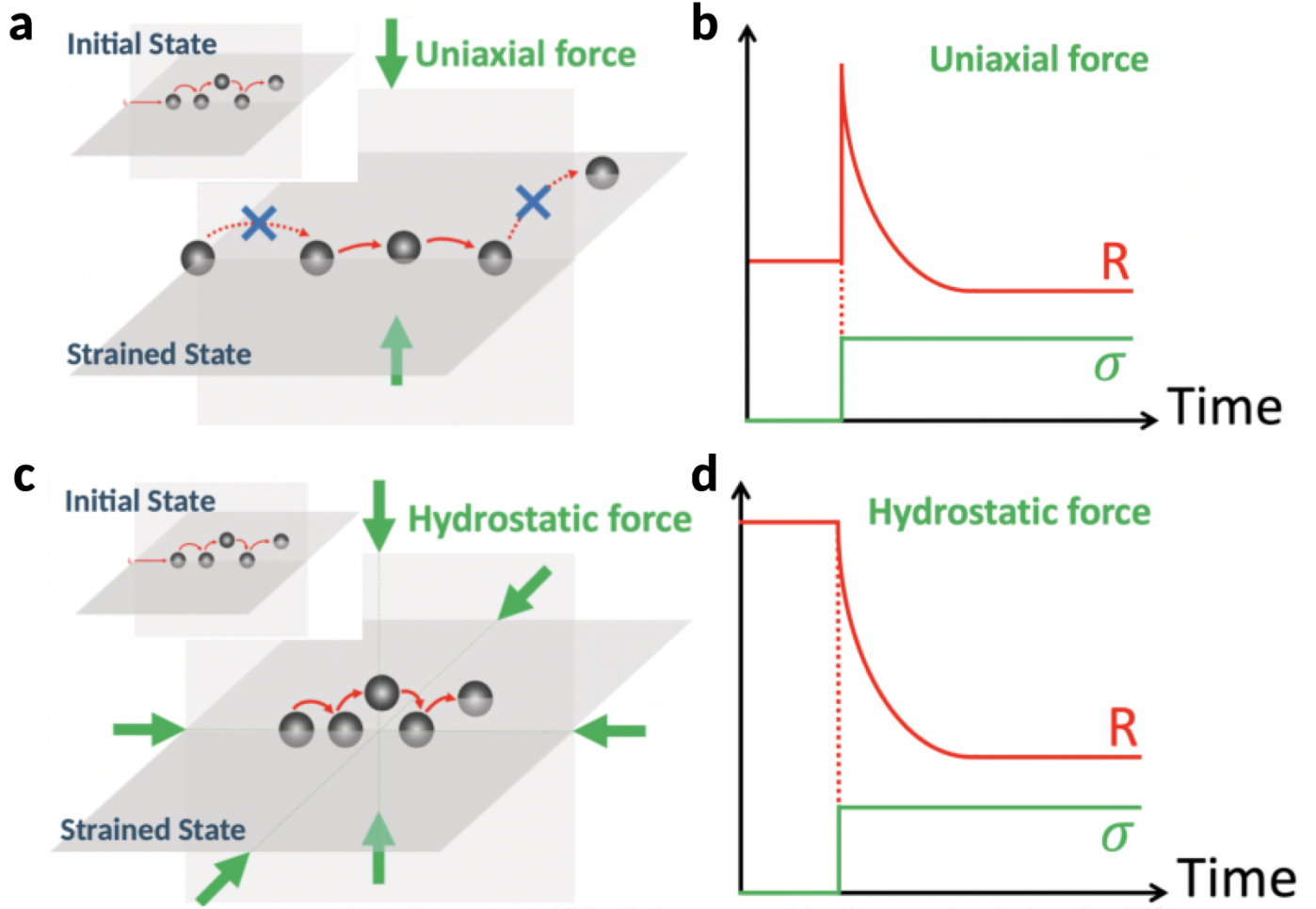
Figure 1: **(a)** Changes in sequential tunnelling resulting from the application of a uniaxial compressive force. *Inset*: percolation path before the application of the force. **(b)** When the composite is subjected to a uniaxial compressive force, the length of tunnelling bonds in the transverse direction instantaneously increases causing a resistance spike. Visco-elastic relaxation then equalizes inter-particle distances and the resistance stabilizes to a new lower value. **(c)** Changes in sequential tunnelling resulting from the application of a hydrostatic force. *Inset*: percolation path before the application of the force. **(d)** When the composite is subjected to a hydrostatic force, the length of the tunnelling bonds in all directions instantaneously decreases causing a monotonical decrease in resistance at the visco-elastic rate.

diameter wire and solder the wire onto the pad. The graphite-PDMS composite was then deposited onto the PCB and moulded into a Hall bar-shaped film of thickness 200μm using an extrusion mask. Two different designs (Figs.2a,c) were trialed for the composite allowing four-terminal resistance measurements to be made. The first design contained six contacts across a straight Hall bar with three pairs of contacts on each side (Figs.2a,b). The current I_{14} flows in the composite through contact 1 and out through contact 4. The voltage across the composite was measured either across contacts 2 and 3 (V_{23}) or across the contacts 6 and 5 (V_{65}). The second design was a L-shaped Hall bar designed to measure simultaneously both local strain components transverse to the applied stress (Fig.2c). In this design, the current I_{15} flows in the composite through contact 1 and out through contact 5. Changes

in piezoresistance induced by one vector component of the transverse strain was detected across contacts 2 and 3 (V_{23}) and the other across contacts 3 and 4 (V_{34}). After a curing time of 48 hours, the composite film was extruded from the mould. For the purpose of reducing the contact resistances of the sensors and to minimize electrical noise, a thin layer of gold was deposited on top of both the composite and copper contact pads. Eventually, the PCB board was diced to form individual sensor elements, 10mm × 10mm each. The composite is bonded to the semi-rigid PCB which realizes the mechanical boundary conditions of the visco-elastic model of the piezoresistance. The top surface of the sensor is in contact with the host material and is free to conform to its granularity and to pick up local strain. Sensors were connected to the remote electrical measurement apparatus. The contact resistance was $\sim 100\Omega$.

3.2. Embedding and loading of the sensors in construction materials

Graphite-PDMS composite strain sensors were embedded in calcium aluminate mortar and Portland cement mortar. The calcium aluminate mortar and Portland cement mortar had a modulus of elasticity of about 0.3GPa and 1GPa, respectively. Furthermore, for comparison purposes, we also embedded our sensors in very fine sand columns to study their response to hydrostatic strain. Very fine sand being fluid, no micro-cracking was expected to occur during stress cycles. The three test samples were fabricated as follows. About 145g of calcium aluminate mortar (sample A) was obtained by mixing 24.16g of water, 13.07g of calcium aluminate cement, 23.67g of CEM I grade cement, 12.75g of pulverized fuel ash, 69.04g of kiln dried sand, 0.49g of plasticiser and 0.74g of accelerator. The Portland cement mortar (sample B) was obtained by mixing water, Portland cement, sand and <5mm grit at a 0.65:1:1:2 ratio. Play sand with grain size 0.2mm-0.5mm was used as very fine sand (sample C).

Samples A were cylindrical blocks 25mm in diameter and 14mm in height with a L-shaped Hall bar composite sensor (Fig.2c) horizontally embedded mid-height. Samples B were cylindrical blocks 39mm in diameter and 60mm in height with a six-contacts Hall bar composite sensor (Figs.2a,b) horizontally embedded mid-height as illustrated in Fig.2d,e. Samples C were very fine sand columns prepared in a steel tube of internal diameter 69mm and height 140mm at the centre of which a single L-shaped Hall bar composite sensor (Fig.2c) was mounted.

Sample labels A1 and A2 correspond to two nominally identical columns of sample type A. Similar notation is used for samples B and C. The notation V_{23} (A1) refers to the piezoresistance of sample A1 measured across probes 2 and 3 (Fig.2c). Likewise, the notations V_{34} (A1), V_{23} (A2), V_{34} (A2), V_{23} (C1), V_{34} (C1), V_{23} (C2) and V_{34} (C2) are used to identify the relevant voltage probes and samples.

3.3. Piezoresistance monitoring and stress-strain measurement

We measured the piezoresistance by injecting a d.c. current $\sim 100\mu$A through the composite Hall bar (Fig.2f). This current provided an optimal signal to noise ratio without generating significant Joule's heating. Noise was filtered by a low pass RC filter with a 10Hz cutoff frequency.
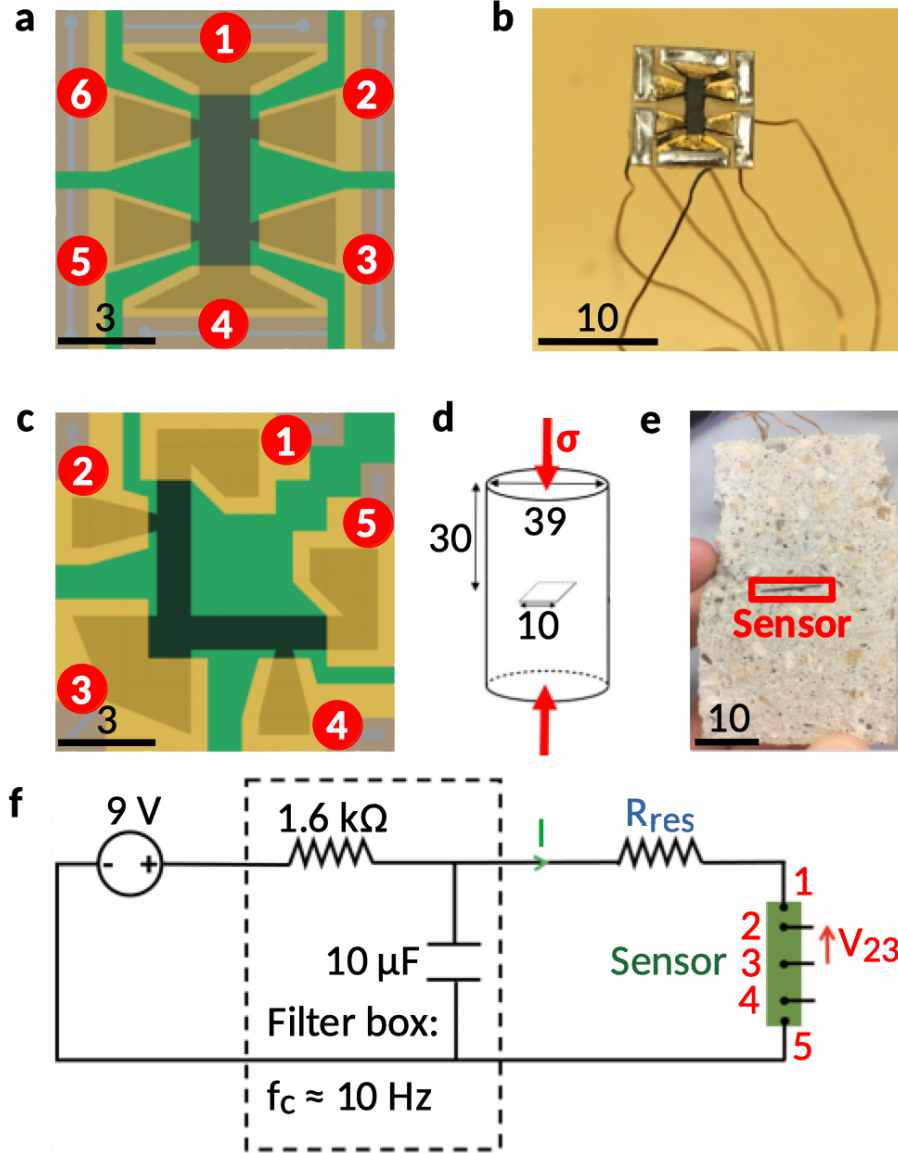
Figure 2: **(a)** Linear design of the graphite-PDMS composite sensors. The active central part of the device consists of a graphite-PDMS Hall bar (black) extending into lateral probes which are contacted with a layer of gold (dark yellow). These lateral probes sit on copper pads which are also covered with the gold layer (light yellow). The copper pads are insulated from each other by the bare printed circuit board (green) and are soldered to electrical wires (grey) connecting the measurement circuit. Voltages V_{23} and V_{65} are measured across the contact pads 2,3 and 6,5 respectively. **(b)** Graphite-PDMS composite sensor post-fabrication showing the composite (black) on the bare PCB (yellow). **(c)** L-shaped design of the graphite-PDMS composite sensor capturing simultaneously both local strain components perpendicular to the applied stress. The colour code used is the same as in (a). **(d)** Schematics of axial compression loading. The red arrows indicate the applied stress. **(e)** Photo of the cross section of a Portland cement mortar block (sample B) taken after test. The irregularities of the side edges result from damage occurring during testing. **(f)** Schematics of the measurement circuit where I is the current driven through the sensor after filtering by a low pass RC filter. This current is controlled by the series resistor $R_{res} = 6.76\text{k}\Omega$. Dimensions are in millimetres.

We monitored the piezoresistance by recording the voltage induced across probes V_{23}, V_{34} or V_{65} using a USB-6211 data acquisition card from National Instruments. The same card was also used to bias the circuit and measure voltage V_{res} across the series resistor. The samples containing the wired sensors were loaded by a Instron 3369 50kN testing frame for monotonic axial compression loading. Applied load/displacement data were recorded with Instron Bluehill 3 control and data acquisition software. The monotonic axial compression loading experiments were carried out at a loading rate of 0.05mm/min and load/displacement data were recorded at a 1Hz sampling frequency.

The four-terminal resistance recorded across probes V_{ij} was calculated as $R_{ij} = R_{res}V_{ij}/V_{res}$ where $R_{res} = 6.76\text{k}\Omega$. The piezoresistance $(R_{ij} - R_0)/R_0$ was then computed as the change in resistance relative to the resistance of the unstrained device, R_0. In rigid materials, stress was communicated axially to the sensor, whereas in sand it was isotropically distributed (Fig.3).
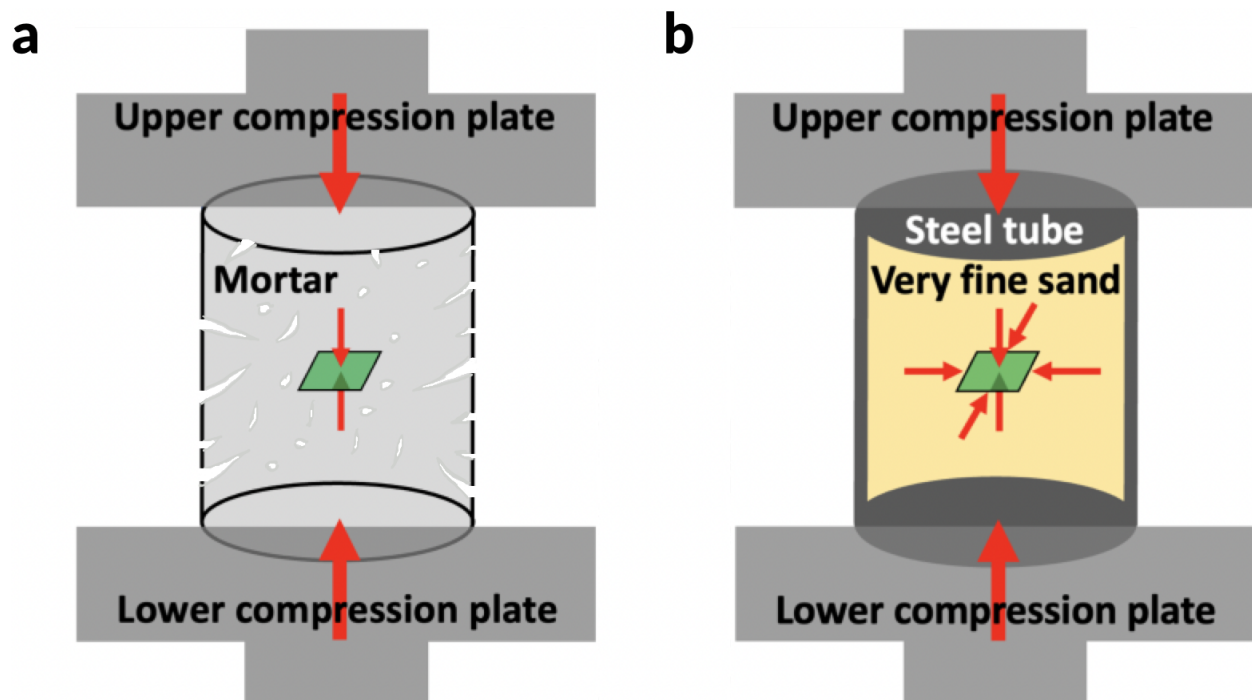

Figure 3: Schematics of the forces (red arrows) being transmitted from the universal testing machine to the column and its embedded sensor. **(a)** Mortar columns consisting of either calcium aluminate or Portland cement. In this case, micro-cracking and cracking may occur. **(b)** Very fine sand column. In this case, neither cracking nor micro-cracking is expected to occur.

3.4. Extraction of strain from the piezoresistance

In order to convert piezoresistance readings into local strain ε_{loc}, we first computed the calibration curve of the piezoresistive film from the tunnelling-percolation piezoresistance formula published by Taylor-Harrod et al. [11]. The strain magnitudes remained in the range 0 - 1.0% where it is known that the theory is in good agreement with the piezoresistance

7

of composite thin films of same filling fraction [10]. Because the applied strains remain small, the model developed for bent substrates remains valid for the present devices under uniaxial compression. The theoretical calibration curve computed from the model is shown in Fig.4b. We compare this curve to the experimental piezoresistance of a composite sensor embedded in Portland cement mortar as a function of the strain measured by an external gauge ε_{avg}, (Fig.4a). Because the piezoresistance responds to changes in strain on the scale of the sensor, the latter strain is the local strain, ε_{loc}. We then used the theoretical calibration curve (Fig.4b) to extract the local strain from the measured piezoresistance of the composite. This conversion of the piezoresistance into local strain produced the local strain dependence on the average strain which is plotted in Figs.5 and 6.
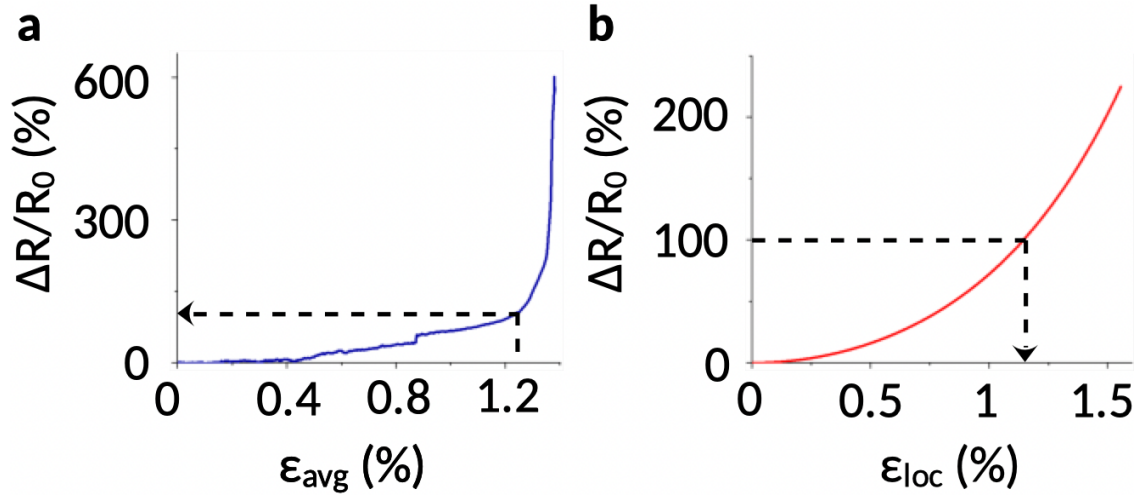

Figure 4: Dependence of the piezoresistance of the composite film on uniaxial strain **(a)** as measured in Portland cement mortar (sample B) and **(b)** as theoretically predicted. ε_{avg} is the macroscopic strain measured by the strain gauge of the universal testing machine.

4. Results

Fig.5 shows the dependence of the local strain on the average strain in the two calcium aluminate mortar samples (samples A). Under axial compression loading, the local strain ε_{loc} increases broadly linearly with the average strain ε_{avg}. The piezoresistive film has a gauge factor of 8. The linear dependence of ε_{loc} on ε_{avg} in different calcium aluminate samples (Fig.5) and across different sensors demonstrates the reproducibility of the sensor responses. In addition, the sensor pair V_{23} and V_{34} mounted at right angles (Fig.2c) detects a fine structure of kinks in ε_{loc} which occur at the same time but vary in opposite direction. These events are labelled α, β, γ, δ and θ in Fig.5. The opposite change in ε_{loc} suggests an abrupt redistribution of strain from one direction to another at each kink. Similar kinks appear in the two Portland cement mortar samples (Fig.6).

We show the stress-strain curves of both calcium aluminate and Portland mortar columns in the insets to Figs.5 and 6. The transition from elastic deformation to plastic deformation occurs at the point where the stress-strain curve saturates. For example, the stress curve of Portland mortar starts flattening at $\sim 1\%$ strain indicating the onset of the plastic phase (inset to Fig.6). The onset of plastic deformation occurs much later in calcium aluminate (inset to Fig.5). A comparison with the stress-strain curves suggests that the kinks observed in the local strain in Figs.5 and 6 take place in the elastic phase prior to irreversible deformation.

The sensor response in cements may be compared to the sensor response in fine sand columns under the same loading conditions (Fig.7). The piezoresistive responses of all 2×2 sensors in L-shaped Hall bars were found to vary completely smoothly under stress. No kink or kink structure was observed in any trace. Instead of the monotonical increase in piezoresistance seen in mortars (Fig.4), we find that the piezoresistance monotonically decreases according to the response expected from hydrostatic pressure (Fig.1d). The two signals V_{23} and V_{34} recorded at a 90 degrees angle nearly superimpose confirming the hydrostatic nature of stress and the reproducibility of sensor readings (Fig.7).
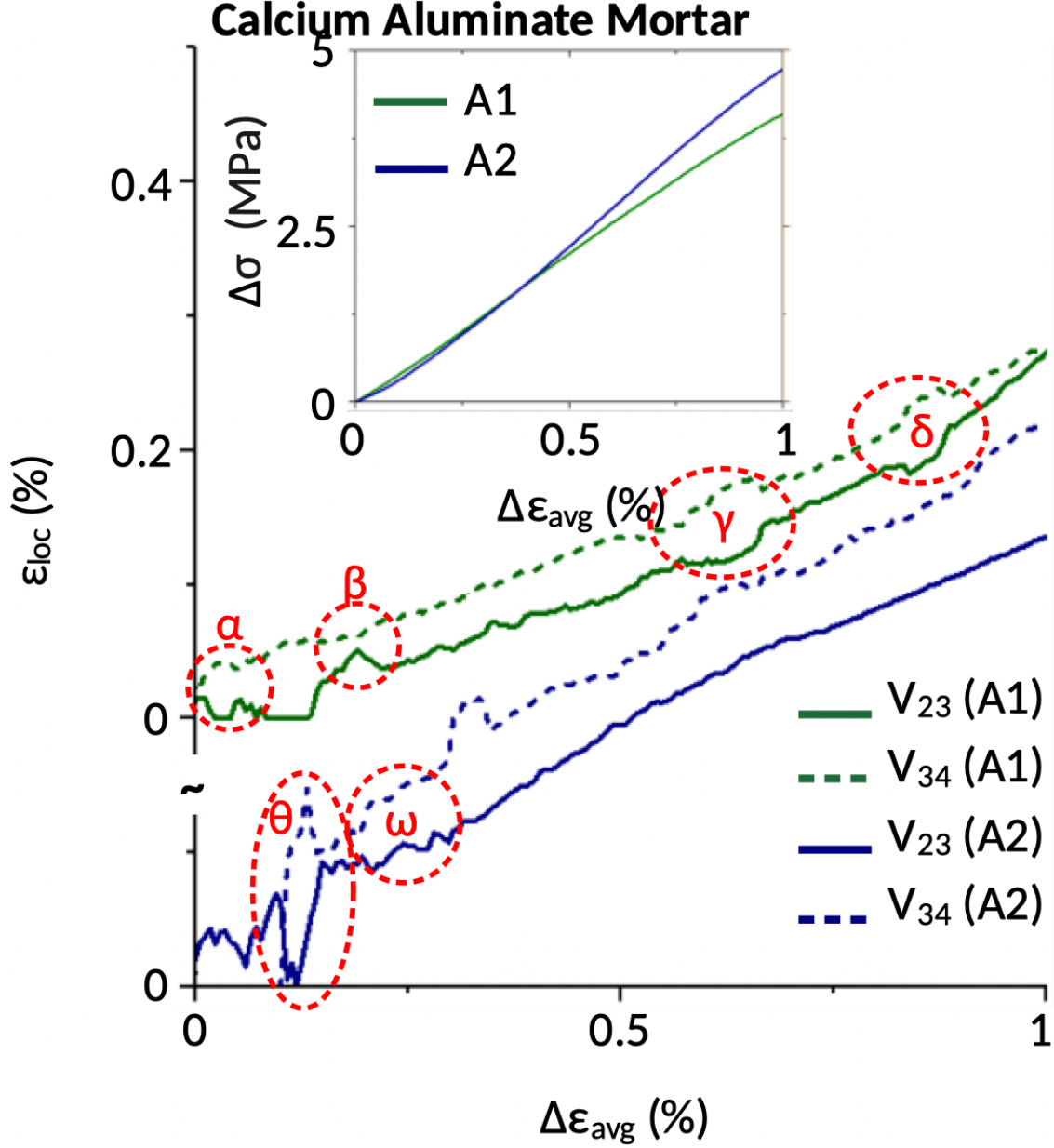
Figure 5: Monotonic axial compression loading of two nominally identical columns of calcium aluminate mortar (samples A1 and A2). The strain ε_{loc} was evaluated by the embedded sensor and plotted as a function of $\Delta\varepsilon_{avg}$ obtained from the strain gauge of the universal testing machine. The strain $\Delta\varepsilon_{avg}$ was corrected for the offset distance before contact between the column and upper compression plate of the universal testing machine is established. V_{23} corresponds to the local strain induced piezoresistance measured between electrode 2 and 3. Similar notation is used for the local strain signals obtained from measurements between electrode 3 and 4. *Inset:* stress-strain curves of samples A1 and A2 measured at the top of the columns by the universal testing machine.

5. Discussion

The kinks observed in the concurrent recordings of local strain signals in calcium alumi-nate mortar (Fig.5) and Portland cement mortar (Fig.6) suggest that micro-cracking might
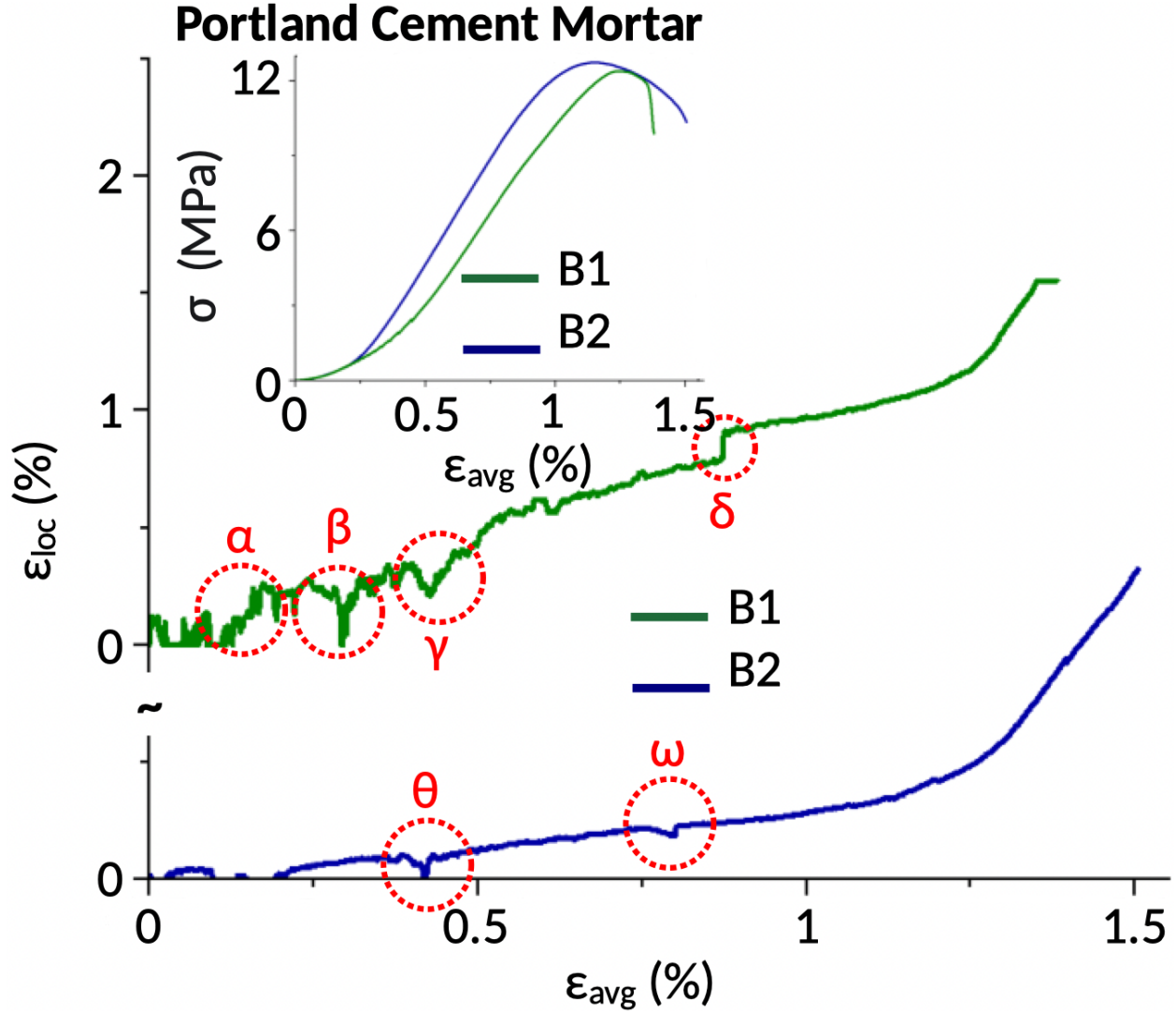
Figure 6: Monotonic axial compression loading of two nominally identical columns of Portland mortar (samples B1 and B2). The local strain ε_{loc} was measured by the embedded sensor and plotted against the macroscopic strain ε_{avg} obtained from the strain gauge of the universal testing machine. *Inset*: stress-strain curves of samples B1 and B2 measured at the top of each block by the universal testing machine.

be occurring during elastic deformation, that is to say before the onset of cracking and irreversible damage. This is validated by the piezoresistive response of our composite sensors in very fine sand subjected to the same uniaxial loading (Fig.7). The smoothness in the sand columns is indeed coherent with hydrostatic transmission of strain (Fig.1d) and the fluid-like nature of this environment, which is not expected to induce micro-cracking and thus piezoresistance kinks. These findings demonstrate that our sensors detect local strain discontinuities in calcium aluminate mortar and Portland cement mortar.

Furthermore, the local strain signals in calcium aluminate mortar (Fig.5) all share the same overall dependence on the average strain and likewise in Portland cement mortar (Fig.6). This suggests that the strain sensing of our composite sensors is very consistent.
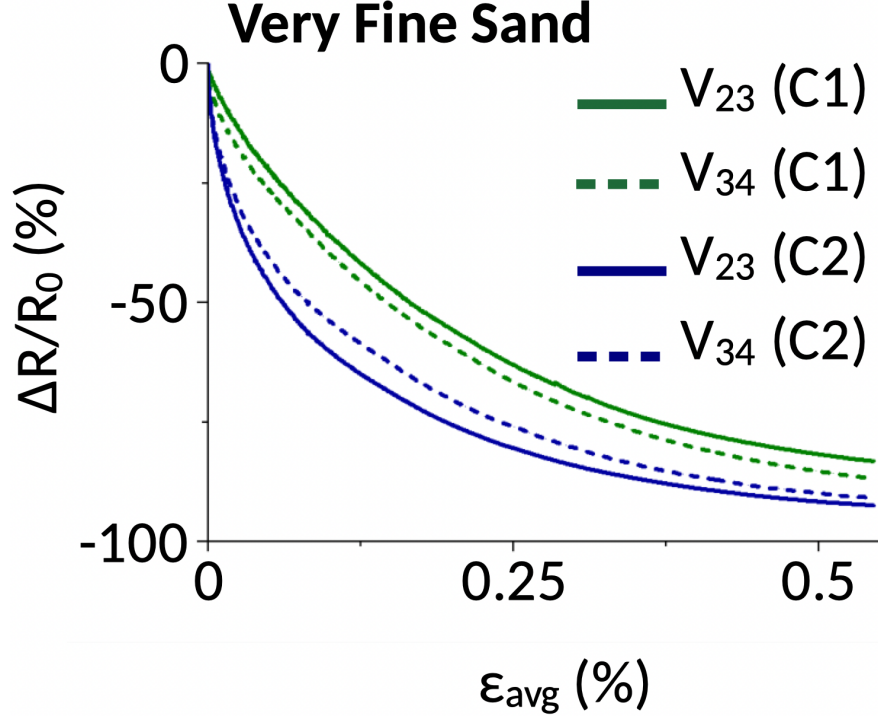
Figure 7: Piezoresistance measured across the L-shaped sensors embedded in the two sand columns (samples C1 and C2). ε_{avg} corresponds to the macroscopic strain obtained from the strain gauge of the universal testing machine. V_{23} and V_{34} are the probes used to measure $\Delta R/R_0$.

The piezoresistive responses (Fig.7) observed at an angle of 90 degrees (L-shaped Hall bar) in very fine sand nearly superimposing for each sensor further confirms the great consistency in the strain sensing of our composite sensors. This consistency is also validated by the piezoresistive responses of both sensors in very fine sand (Fig.7) sharing the same overall completely smooth monotonic decrease. This completely smooth monotonic decrease is consistent with the hydrostatic hypothesis (Fig.1d) for our sand columns.

In addition, the opposite kinks in the local strain signals in calcium aluminate mortar (Fig.5) observed at an angle of 90 degrees (L-shaped Hall bar) suggests that the strain might have been relaxed in the material through redistribution from one axis to another via the formation of micro-cracks. This is validated by the identical local strain signals in very fine sand (Fig.7) observed at an angle of 90 degrees (L-shaped Hall bar) where no cracking is expected to occur. The responses of our sensors in calcium aluminate mortar are thus consistent with stress buildup relaxing from one transverse direction to another.

Lastly, the local strain increasing faster in Portland cement mortar (Fig.6) than in calcium aluminate mortar (Fig.5), is consistent with the fact that Portland cement mortar has a higher Young's modulus than calcium aluminate mortar. The higher Young's modulus of Portland cement mortar over calcium aluminate mortar is indeed reflected in the plastic phase being reached at a higher value of the applied stress in Portland cement mortar (inset of Fig.5) than in calcium aluminate mortar (inset of Fig.6).

The composite elastomer may be scaled down to the size of graphitic nanoparticles

(450nm) without significant modification in the sensor performance. Such devices would likely be fabricated using imprint lithography rather than moulding. Hall channels narrower than 1μm would however host a reduced number of percolation paths. In this limit, the piezoresistance is expected to become dependent of the arrangement of nanoparticles, hence fluctuate from device to device. Alternatively carbon nanotubes could be used as filler [19, 24, 25] with advantages in reducing fatigue under repeated stress-strain cycles. HOPG nanoparticles however tend to form bundles and with average lengths of a few tens of microns are less amenable to scaling piezoresistive devices. We have not used and do not expect a protective layer to be needed between the sensor and the embedding material. This is because PDMS is chemically stable with depolymerization starting above 400°. At room temperature, degradation is known to occur through hydrolysis in the presence of sunlight. This is not expected to affect sensors embedded in concrete or other structural materials.

6. Conclusions

Our work has demonstrated novel piezoresistive sensors that may be embedded inside cementitious materials and are sufficiently small to detect the onset of cracking on the millimeter scale. The sensors rely on the tunnelling-percolation mechanism to detect minute changes in strain ($< 0.1\%$). They detect displacements of a few tens of microns and have a gauge factor of 8, whereas polysilicon have a gauge factor of ~ 100, and sensitivity of $\sim 0.1\%$. The graphite-PDMS rubber, which we have demonstrated here, is a cheap material. It is ideally suited to making large scale arrays of millions of sensors to be distributed across cementitious structures to monitor structural health and to perform sonic tomography.

7. Competing interests

The authors declare no competing interests.

8. Author contributions

AVG built the sensors and performed experiments. RB conceived the experiments concrete samples. AN designed the project and secured funding. All authors contributed to writing the manuscript.

9. Acknowlegments

References

[1] Y. Gao, G. Y. Tian, P. Wang, H. Wang, B. Gao, W. L. Woo, K. Li, Electromagnetic pulsed thermography for natural cracks inspection, Scientific reports 7 (2017) 42073.

[2] H. Taha, R. J. Ball, K. Paine, Sensing of damage and repair of cement mortar using electromechanical impedance, Materials 12 (23) (2019) 3925.

[3] W. Li, B. Dong, Z. Yang, J. Xu, Q. Chen, H. Li, F. Xing, Z. Jiang, Recent advances in intrinsic self-healing cementitious materials, Advanced Materials 30 (17) (2018) 1705679.

[4] K. Davami, M. Mohsenizadeh, M. Mitcham, P. Damasus, Q. Williams, M. Munther, Additively manufactured self-healing structures with embedded healing agent reservoirs, Scientific reports 9 (1) (2019) 7474.

[5] R. R. Menon, J. Luo, X. Chen, H. Zhou, Z. Liu, G. Zhou, N. Zhang, C. Jin, Screening of fungi for potential application of self-healing concrete, Scientific reports 9 (1) (2019) 2075.

[6] W. Pungrasmi, J. Intarasoontron, P. Jongvivatsakul, S. Likitlersuang, Evaluation of microencapsulation techniques for micp bacterial spores applied in self-healing concrete, Scientific reports 9 (1) (2019) 1–10.

[7] S. Gupta, G. Vella, I.-N. Yu, C.-H. Loh, W.-H. Chiang, K. J. Loh, Graphene sensing meshes for densely distributed strain field monitoring, Structural Health Monitoring (2019) 1475921719877418.

[8] J. Zhang, G. Y. Tian, A. M. Marindra, A. I. Sunny, A. B. Zhao, A review of passive rfid tag antenna-based sensors and systems for structural health monitoring applications, Sensors 17 (2) (2017) 265.

[9] W. Ostachowicz, R. Soman, P. Malinowski, Optimization of sensor placement for structural health monitoring: A review, Structural Health Monitoring 18 (3) (2019) 963–988.

[10] A. S. Chauhan, I. Taylor-Harrod, S. D. Littlejohn, A. Nogaret, Ultrafast pressure sensing with transient tunnelling currents, Nanoscale 9 (13) (2017) 4544–4549.

[11] I. Taylor-Harrod, A. Nogaret, Piezoresistance of flexible tunneling-percolation networks, Physical Review B 96 (2) (2017) 024205.

[12] R. M. Negri, S. D. Rodriguez, D. L. Bernik, F. V. Molina, A. Pilosof, O. Perez, A model for the dependence of the electrical conductance with the applied stress in insulating-conducting composites, Journal of Applied Physics 107 (11) (2010) 113703.

[13] S. Littlejohn, A. Nogaret, G. M. Prentice, G. D. Pantos, Pressure sensing and electronic amplification with functionalized graphite–silicone composite, Advanced Functional Materials 23 (43) (2013) 5398–5402.

[14] T. Someya, T. Sekitani, S. Iba, Y. Kato, H. Kawaguchi, T. Sakurai, A large-area, flexible pressure sensor matrix with organic field-effect transistors for artificial skin applications, Proceedings of the National Academy of Sciences 101 (27) (2004) 9966–9970.

[15] D. Son, J. Kang, O. Vardoulis, Y. Kim, N. Matsuhisa, J. Y. Oh, J. W. To, J. Mun, T. Katsumata, Y. Liu, et al., An integrated self-healable electronic skin system fabricated via dynamic reconstruction of a nanostructured conducting network, Nature nanotechnology 13 (11) (2018) 1057.

[16] J. Y. Oh, D. Son, T. Katsumata, Y. Lee, Y. Kim, J. Lopez, H.-C. Wu, J. Kang, J. Park, X. Gu, et al., Stretchable self-healable semiconducting polymer film for active-matrix strain-sensing array, Science advances 5 (11) (2019) eaav3097.

[17] C. Hou, T. Huang, H. Wang, H. Yu, Q. Zhang, Y. Li, A strong and stretchable self-healing film with self-activated pressure sensitivity for potential artificial skin applications, Scientific reports 3 (2013) 3138.

[18] G. Liu, D. Kong, S. Hu, Q. Yu, Z. Liu, T. P. Chen, Y. Yin, S. Hosaka, Y. Liu, Smart electronic skin having gesture recognition function by lstm neural network, Applied Physics Letters 113 (8) (2018) 084102.

[19] D. J. Lipomi, M. Vosgueritchian, B. C. Tee, S. L. Hellstrom, J. A. Lee, C. H. Fox, Z. Bao, Skin-like pressure and strain sensors based on transparent elastic films of carbon nanotubes, Nature nanotechnology 6 (12) (2011) 788.

[20] C. S. Boland, U. Khan, C. Backes, A. O'Neill, J. McCauley, S. Duane, R. Shanker, Y. Liu, I. Jurewicz, A. B. Dalton, et al., Sensitive, high-strain, high-rate bodily motion sensors based on graphene–rubber composites, ACS nano 8 (9) (2014) 8819–8830.

[21] C. S. Boland, U. Khan, G. Ryan, S. Barwich, R. Charifou, A. Harvey, C. Backes, Z. Li, M. S. Ferreira, M. E. Möbius, et al., Sensitive electromechanical sensors using viscoelastic graphene-polymer nanocomposites, Science 354 (6317) (2016) 1257–1260.

[22] L. Chen, G. Chen, L. Lu, Piezoresistive behavior study on finger-sensing silicone rubber/graphite nanosheet nanocomposites, Advanced Functional Materials 17 (6) (2007) 898–904.

[23] S. C. Mannsfeld, B. C. Tee, R. M. Stoltenberg, C. V. H. Chen, S. Barman, B. V. Muir, A. N. Sokolov, C. Reese, Z. Bao, Highly sensitive flexible pressure sensors with microstructured rubber dielectric layers, Nature materials 9 (10) (2010) 859.

[24] S. Luo, G. Wang, Y. Wang, Y. Xu, Y. Luo, Carbon nanomaterials enabled fiber sensors: A structure-oriented strategy for highly sensitive and versatile in-situ monitoring of composite curing process, Composites Part B: Engineering 166 (2019) 645–652.

[25] B. Hao, Q. Ma, S. Yang, E. Mäder, P.-C. Ma, Comparative study on monitoring structural damage in fiber-reinforced polymers using glass fibers with carbon nanotubes and graphene coating, Composites Sciences and Technology 129 (2016) 38–45.

[26] J. M. López-Higuera, L. R. Cobo, A. Q. Incera, A. Cobo, Fiber optic sensors in structural health monitoring, Journal of lightwave technology 29 (4) (2011) 587–608.

[27] Y. Saito, H. Takao, T. Tani, T. Nonoyama, K. Takatori, T. Homma, T. Nagaya, M. Nakamura, Lead-free piezoceramics, Nature 432 (7013) (2004) 84–87.

[28] E. Cross, Lead-free at last, Nature 432 (7013) (2004) 24–25.

[29] E. Aksel, J. L. Jones, Advances in lead-free piezoelectric materials for sensors and actuators, Sensors 10 (3) (2010) 1935–1954.

[30] C. Grimaldi, I. Balberg, Tunneling and nonuniversality in continuum percolation systems, Physical Review Letters 96 (2006) 066602.

[31] S. Littlejohn, A. Nogaret, S. Crampin, Tunneling negative differential resistance in a flexible active composite, Advanced Materials 23 (25) (2011) 2815–2818.